

PULSED NEUTRON DIFFRACTION IN SPECIAL SAMPLE ENVIRONMENTS*

J. D. Jorgensen
Materials Science Division
Argonne National Laboratory
Argonne, IL 60439

ABSTRACT. Neutron diffraction is a powerful tool for structural studies of samples in special sample environments because of the high penetrating power of neutrons compared to X-rays. The neutrons readily penetrate special sample containers, heat shields, pressure vessels, etc., making it unnecessary in most cases to compromise the effectiveness of the sample environment system by providing windows for the incident and scattered neutrons. Pulsed neutrons obtained from an accelerator-based pulsed neutron source offer the additional advantage that many diffraction experiments can be done at a single, fixed scattering angle by the time-of-flight technique. Thus, if windows are needed (e.g., in an especially thick-walled sample vessel such as a pressure cell), they need to cover only a limited angular range. More importantly, in the fixed-angle scattering geometry, shielding and collimation can be optimized in order to access the largest possible sample volume with neutrons while completely avoiding scattering from the surrounding sample vessel. Thus, the data are free from unwanted background scattering which could hamper data interpretation. In this paper, the basic principles of neutron diffraction in special sample environments are discussed and examples of apparatus used for neutron diffraction measurements at low temperature, high temperature, and high pressure are presented. The concepts are illustrated with several unique scientific results taken from the published literature.

1. INTRODUCTION

At the present time the majority of neutron scattering experiments are done under special sample environment conditions. Refrigerators, cryostats, furnaces, and pressure cells are used routinely at all of the major neutron scattering centers for both elastic and inelastic neutron

*Work supported by the U. S. Department of Energy, BES-Materials Sciences, under contract W-31-109-ENG-38.

scattering experiments.¹ Using proper experimental techniques the quality of data for a sample in a cryostat, furnace, or pressure cell can be equivalent to what would be obtained at room temperature and atmospheric pressure.

The ability to perform neutron scattering experiments in special environments is a result of the high penetrating power of the neutron. Because the neutron is a neutral particle and because the total cross section (scattering plus absorption) is rather low for most materials, scattering experiments can easily be done in geometries where the sample is contained in heat shields, pressure cells, reaction vessels, etc., through which the incident and scattered neutrons must pass. For typical thin aluminum heat shields the neutron attenuation is negligible. For thicker sample containers such as aluminum or aluminum oxide pressure cells, the overall attenuation may be on the order of 50% for a vessel with 1 cm-thick walls.

1.1. Advantages of Pulsed Neutrons for Diffraction in Special Sample Environments

Pulsed neutron sources offer the additional advantage that complete data can be obtained at a single, fixed scattering angle by the time-of-flight technique.^{2,3} Thus, if it is necessary to provide windows for the incident and scattered neutrons in a particularly restrictive sample vessel (e.g., a large pressure cell), the windows need to cover only a limited angular range. Furthermore, the scattering angle can be chosen so that shielding and collimation can be optimized to provide the maximum effective sample volume while eliminating unwanted scattering from the sample vessel.

1.2. Experimental Geometry for Diffraction in Special Environments

The goal of any special environment apparatus for neutron diffraction is to provide clean diffraction data (i.e., data free from unwanted scattering from the sample vessel) while achieving the desired sample conditions (temperature, pressure, etc.). Virtually all special sample environments used at pulsed neutron sources are extensions of the two basic geometries shown in Fig. 1. These geometries ensure that the sample is the only volume which is seen by both the incident beam and the detector. In Fig. 1(a), the incident and scattered beams are both collimated by a cadmium mask, with windows at selected angles, which surrounds the sample and heat shield. Thus, even though the incident beam passes through and scatters from the aluminum heat shield before and after striking the sample, the detector is prevented from seeing the unwanted scattering. Of course, a small part of the scattered beam is also scattered from the heat shield between the sample and the detector, but this is a second order effect and, moreover, contributes to the smooth background rather than to sharp features in the data. The geometry shown in Fig. 1(a) is most useful when the scattering angle can be chosen to be at or near $2\theta = 90^\circ$, so that the collimation can define a localized sample volume. For larger or smaller angles it becomes

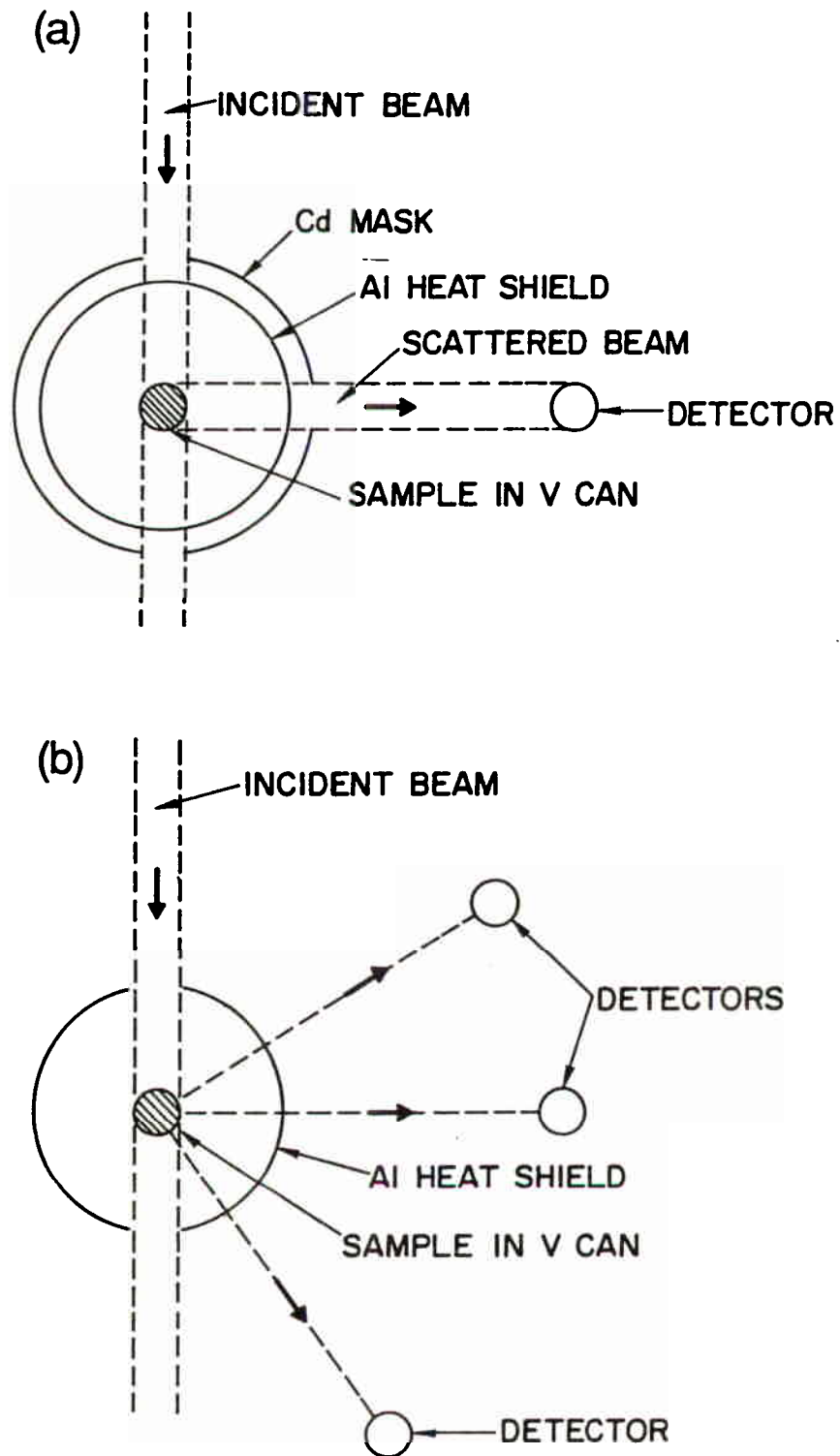


Figure 1. Generalized special environment geometries for time-of-flight diffraction experiments: (a) Collimation of both the incident and scattered beams at a single, fixed scattering angle. (b) The use of windows for the direct beam so that multiple scattering angles can be used.

increasingly more difficult to eliminate scattering from the region surrounding the sample because the probed volume is elongated.

The geometry shown in Fig. 1(b) can be used where small or large scattering angles are needed or where multiple scattering angles are used. Even though a wide range of d spacings can be accessed at a single scattering angle by the time-of-flight technique (e.g., enough data can typically be obtained in back scattering or at $2\theta = 90^\circ$ to perform a Rietveld structural refinement), some experiments demand that the data range be extended further. For example, small scattering angles must be used to measure magnetic reflections at large d spacing or to obtain the largest d spacing nuclear reflections for determination of unknown structures. In the geometry shown in Fig. 1(b), windows are cut in the heat shield before and after the sample so that the incident neutrons strike only the sample. This geometry has been most effectively used at low temperature or in furnaces designed to reach a few hundred degrees C. Since the window does compromise the effectiveness of the heat shield, care must be taken to ensure that the sample (in its container) does not support a thermal gradient and that the sample temperature is measured correctly. In the case of low temperature experiments, the window can often be covered with several layers of aluminized mylar (sometimes called superinsulation) to provide a degree of heat shielding while introducing a negligible amount of scattering material into the incident beam.

Some commonly used materials for sample containment and shielding are listed in Table I. Vanadium is the most commonly used material for sample cans because of its nearly zero coherent cross section. If the walls of the vanadium can are thin (typically less than 0.2 mm) the Bragg peaks from the vanadium will be below the background levels of most experiments. Vanadium has mechanical and thermal conductivity properties similar to stainless steel and can be extruded into tubes and other useful shapes if the starting material is of sufficient purity.

TABLE I. Commonly used materials for neutron diffraction sample containment and shielding

<u>Material</u>	<u>Cross Sections (barns)</u>		<u>Use</u>
	<u>Coherent</u>	<u>Absorption</u>	
V	0.02	5.1	Sample cans
Al	1.50	0.2	Heat shields
Cd	3.3	2,520	Shielding
B	3.54	767	Shielding
Gd	34.5	48,890	Shielding

Reference: Methods in Experimental Physics, Vol. 23-Part A, Neutron Scattering, edited by K. Sköld and D. L. Price (Academic Press, New York 1986) Appendix.

Permanent vacuum-tight joints can be made by electron beam welding of vanadium to stainless steel or titanium, but the seams may not survive thermal cycling since the thermal expansions are not identical. The best vacuum-tight sample cans have beam-welded vanadium end caps. Vanadium has also been used as a heat shield in some furnace designs. However, if the volume of vanadium in the beam becomes excessive, it may become the dominant contribution to the background, due to the nonzero incoherent cross section (5.2 barns). Moreover, since the thermal conductivity of vanadium is rather poor (similar to stainless steel), a thin-walled heat shield can support a sizeable temperature gradient. In at least one furnace design, a thin-walled vanadium tube (surrounding the sample) is used as the heating element.

The most commonly used shielding material is cadmium. The neutron absorption cross section of cadmium is sufficiently large that sheets on the order of 0.5 mm thickness are essentially opaque to thermal neutrons. Cadmium is a soft and malleable metal, similar to lead, and can be easily formed into useful shapes for shielding. Other useful shielding materials (chosen because of their large absorption cross sections) include boron and gadolinium. Boron is typically used in the form of boron nitride (BN), which can be easily machined into useful shapes and will survive high-temperature environments, and boron carbide (B_4C) which is most commonly available as a coarse (and very abrasive) powder but can be mixed with epoxy resin and cast into useful shapes or contained in metal cans for bulk shielding. Gadolinium is often used in the form of fine gadolinium oxide powder mixed with thin epoxy resin and applied as a paint.

Figure 2 shows a possible design for a neutron diffraction sample can which can be sealed. The can is made from a length of thin-walled (approximately 0.1 mm) vanadium tubing with a solid cap on one end and a flange and removable cap on the other. The removable cap can be sealed with either an elastomer or indium O-ring. An indium seal will be effective at low temperature if the cap is designed in such a way that the indium is under compression at all temperatures. In the design shown in Fig. 2, elongation of the small-diameter screws which secure the cap to the flange around its perimeter (combined with a careful choice of thermal expansions) provides the stored mechanical energy which ensures that the indium remains under compression at low temperatures. The design of high-temperature sealed cans can also proceed along similar lines with an appropriate choice of the gasket material.

2. NEUTRON DIFFRACTION AT LOW TEMPERATURE

Perhaps the most common special sample environment used in neutron diffraction is low temperature. Achieving a low sample temperature can be desirable for a number of reasons. In some cases, the purpose is to reduce thermal vibration and thus increase the signal-to-noise ratio of the data by increasing the Bragg intensity while reducing thermal diffuse scattering. Low-temperature data collection can be particularly important in the case of "soft" materials such as organic systems or

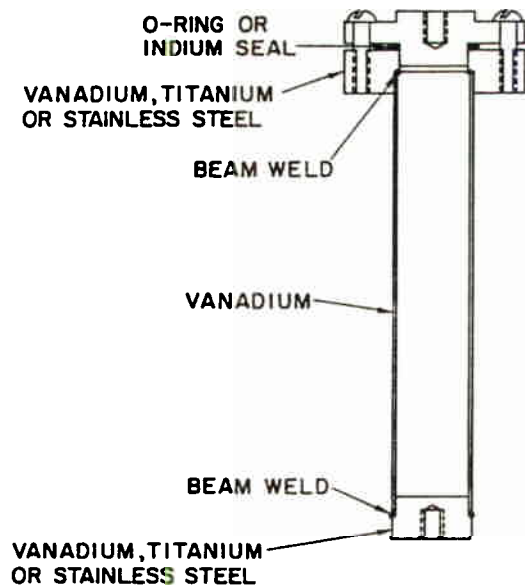


Figure 2. Typical design for a reusable, sealed neutron diffraction sample can.

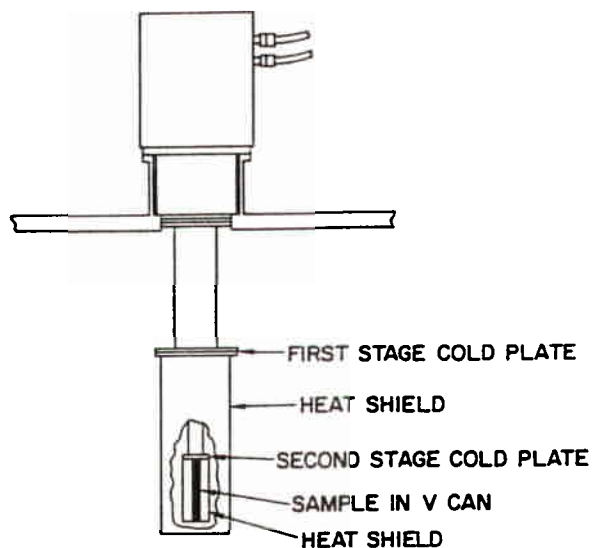


Figure 3. Closed cycle helium refrigerator (Displex) configured for low-temperature neutron diffraction experiments.

systems containing mobile atoms (e.g., metal hydrides) although in some cases, ordering of the mobile species at low temperature may produce a phase transition to a structure different from the one which is of interest.

Another purpose for low temperature data collection is to enable the study of structural or magnetic phase transitions. In many cases, the relevant order parameter for the transition can be studied as a function of temperature to establish the critical exponent.

Since many other interesting physical phenomena occur at low temperature, another common purpose for low temperature data collection is to establish the structure at the same temperature at which other novel behavior is observed. For example, neutron diffraction at low temperature has been used to determine the structures of systems such as solid helium and hydrogen, as well as to establish important correlations between structure and superconductivity in both organic and inorganic compounds.

2.1. Experimental Methods

Virtually all of the techniques employed in low-temperature physics have been successfully applied to neutron diffraction experiments. The

TABLE II. Experimental methods for neutron diffraction at low temperatures.

Method	Min. Temp. (K)
Closed cycle refrigerator (Displex)	10
Helium cryostat	4.2
Pumped helium cryostat: ^4He	1.5
^3He	0.5
^4He - ^3He dilution refrigerator	0.05
Nuclear demagnetization	0.001

cooling method employed depends on the minimum temperature desired. The most commonly used techniques, along with the minimum temperatures that can be achieved, are listed in Table II. The closed-cycle helium refrigerator (Fig. 3) is a particularly convenient technique for temperatures down to 10 K because there is no need for periodic transfer of cryogenic liquids, as is the case for a cryostat. However, a well-designed cryostat may provide shorter cooldown times in cases where the cryostat has been designed for insertion of the sample directly into the cold zone. In both cases, the temperature can be controlled from a computer-based data acquisition system so that data at a series of temperatures can be collected according to a predetermined program without intervention from the experimenter.

If temperatures lower than 4 K are required, pumped helium cryostats (pumped ^4He to 1.5 K and pumped ^3He to 0.5 K) can be used although such systems require more attention while operating. Below 0.5 K, a ^3He - ^4He dilution refrigerator can be employed.⁴ The literature contains a number of important elastic and inelastic neutron scattering experiments in the range of 0.05-4 K involving the use of dilution refrigerators. In particular, these techniques have allowed unique studies of important quantum solid and liquids such as ^3He , ^4He , and H.⁵⁻⁷

Proceeding below about 0.05 K requires the use of a nuclear demagnetization stage in combination with a ^3He - ^4He dilution refrigerator. Neutron scattering experiments have been performed in at least two laboratories with the use of such techniques. The lowest temperature neutron diffraction experiment is a recent study of the nuclear magnetic ordering in solid ^3He at 0.0005 K.⁸ For this experiment, careful attention to the choice of materials in the direct beam was required in order to minimize the neutron and gamma-ray heating effects. Care was also taken to minimize heating due to vibration of the experimental apparatus. Figure 4 shows a nuclear demagnetization system for similar experiments conducted at the Intense Pulsed Neutron Source at Argonne National Laboratory.⁹

2.2. Examples

A number of straightforward examples from the published literature can be used to illustrate some of the basic concepts of pulsed-source time-of-flight neutron diffraction at low temperature.

2.2.1. Mechanism of thermal expansion in α -quartz SiO_2 . On the high resolution powder diffractometer at the ZING prototype pulsed neutron source, a simple study of α -quartz SiO_2 versus temperature was performed in order to demonstrate experimentally that the thermal expansion at low temperature, which is markedly nonlinear below 100 K, could be explained in terms of a rigid rotation of corner-linked SiO_4 tetrahedra.¹⁰ The experimental arrangement used for this experiment (Fig. 5) illustrates some basic concepts which apply to all neutron scattering experiments at low temperature. The powder SiO_2 sample was contained in a helium

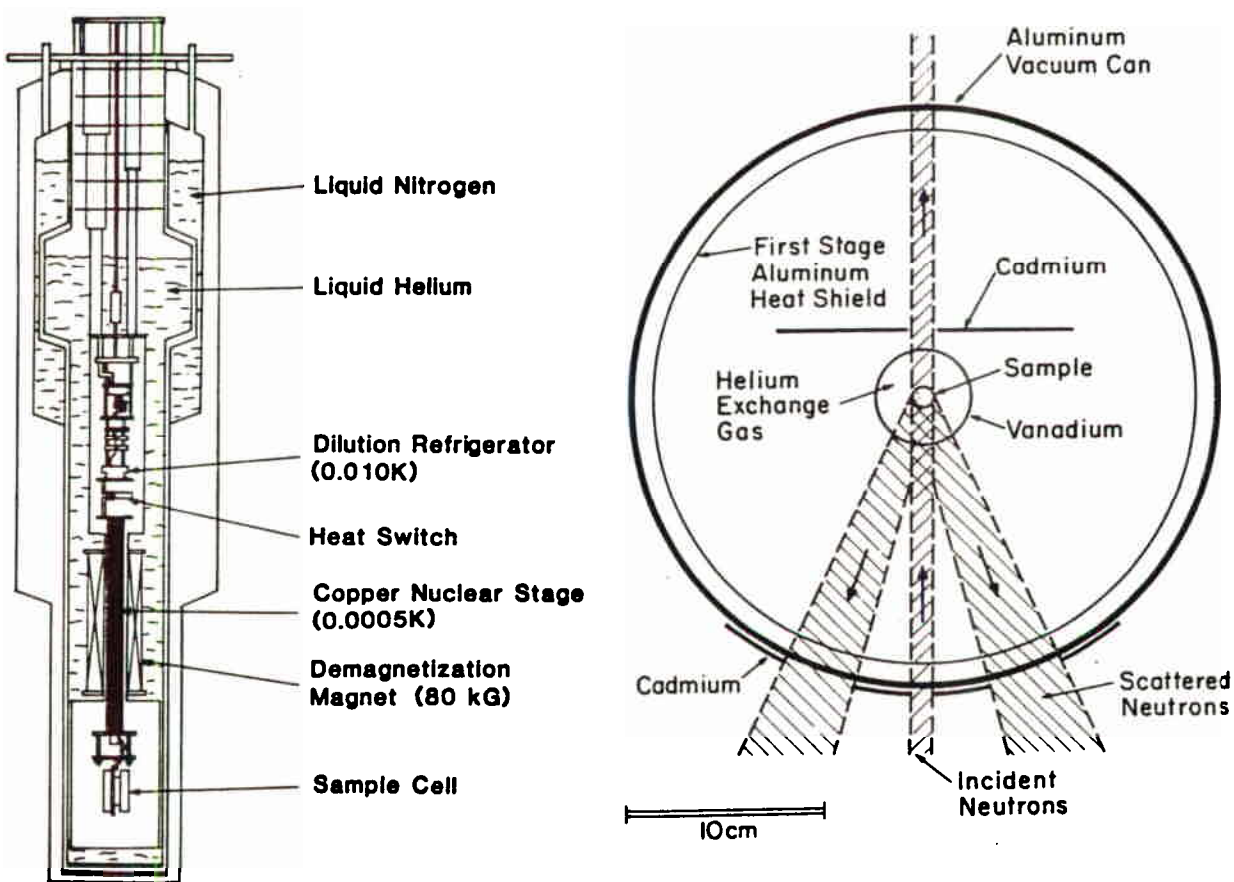


Figure 4. Nuclear demagnetization system used for ultra-low-temperature neutron diffraction measurements at the Intense Pulsed Neutron Source.

Figure 5. Schematic drawing of the experimental arrangement of heat shields and neutron shielding for low-temperature neutron diffraction measurements on a backscattering ($2\theta = 160^\circ$) instrument. (Reproduced from Ref. 10.)

exchange gas to ensure rapid and uniform cooling of the powder particles. Without the use of an exchange gas, it is impossible to ensure that the powder actually cools at the same rate as the sample can and the cold plate to which it is mounted. This is especially true for powders which have poor thermal conductivity at low temperature. Additionally, without the use of an exchange gas, it may not be valid to assume that the thermometer, which is typically mounted to the sample can or cold plate, accurately measures the sample temperature. (It should be remembered that a thin-walled vanadium sample can is capable of supporting a significant temperature gradient.) Uniform cooling of a powder sample can be achieved by containing the sample in a properly sealed (i.e., with an indium seal) vanadium can along with one atmosphere (at room temperature) of helium exchange gas.

2.2.2. Low temperature magnetic structures in FeGe. The study of magnetic structures requires the use of small scattering angles in order to ensure that the large d spacing Bragg peaks which result from the magnetic ordering are seen. The low temperature magnetic structures of FeGe were determined from analysis of data taken by the time-of-flight technique on the Special Environment Powder Diffractometer (SEPD) at IPNS at a scattering angle of $2\theta = 57^\circ$.¹¹ At this scattering angle the SEPD provides data to about 8 Å d spacing at a resolution of $\Delta d/d \approx 1\%$. There are two magnetic ordering transitions of the monoclinic ($z = 6$) structure. At 340 K, some of the Fe atoms order antiferromagnetically to give a cell doubling along the c axis; at 120 K an additional incommensurate modulation of spins along the b direction occurs. Raw time-of-flight neutron data in each of the three phases, with the new magnetic reflections identified, are shown in Fig. 6. For this experiment, even though the decrease in flux at long wavelengths resulted in rather small raw intensities at large d spacing, the 1% resolution available at $2\theta = 57^\circ$ was especially useful in solving the incommensurate structure.

2.2.3. Structural instability and superconductivity in the Chevrel phases (MMo_6S_8). Recent low-temperature neutron diffraction measurements on Chevrel phase compounds with composition MMo_6S_8 ($M = Sn, Pb, Ba, Yb$) have shown a direct relationship between high superconducting transition temperatures (T_c) and structural instability in these compounds.¹² Original structural measurements had shown that the Chevrel phases which exhibited superconductivity (e.g., Sn-, Pb-, and Yb Mo_6S_8) were in a rhombohedral, $R\bar{3}$, structure. It was later discovered that similar compounds which showed no superconductivity (e.g., Ba Mo_6S_8 and Eu Mo_6S_8) transformed to a triclinic, $P\bar{1}$, structure at low temperature. The triclinic distortion destroys superconductivity by splitting a half-filled band and opening a gap at the Fermi energy. The highest T_c Chevrel phase compounds, Sn Mo_6S_8 and Pb Mo_6S_8 , ($T_c \approx 14$ K) had been repeatedly reported to exhibit evidence for structural instability at low temperature based on a wide variety of experimental techniques, but the nature of the low-temperature anomaly was not clear in any of the experiments. (See the references cited in Ref. No. 12). Neutron powder diffraction measurements were recently able to identify the subtle low-

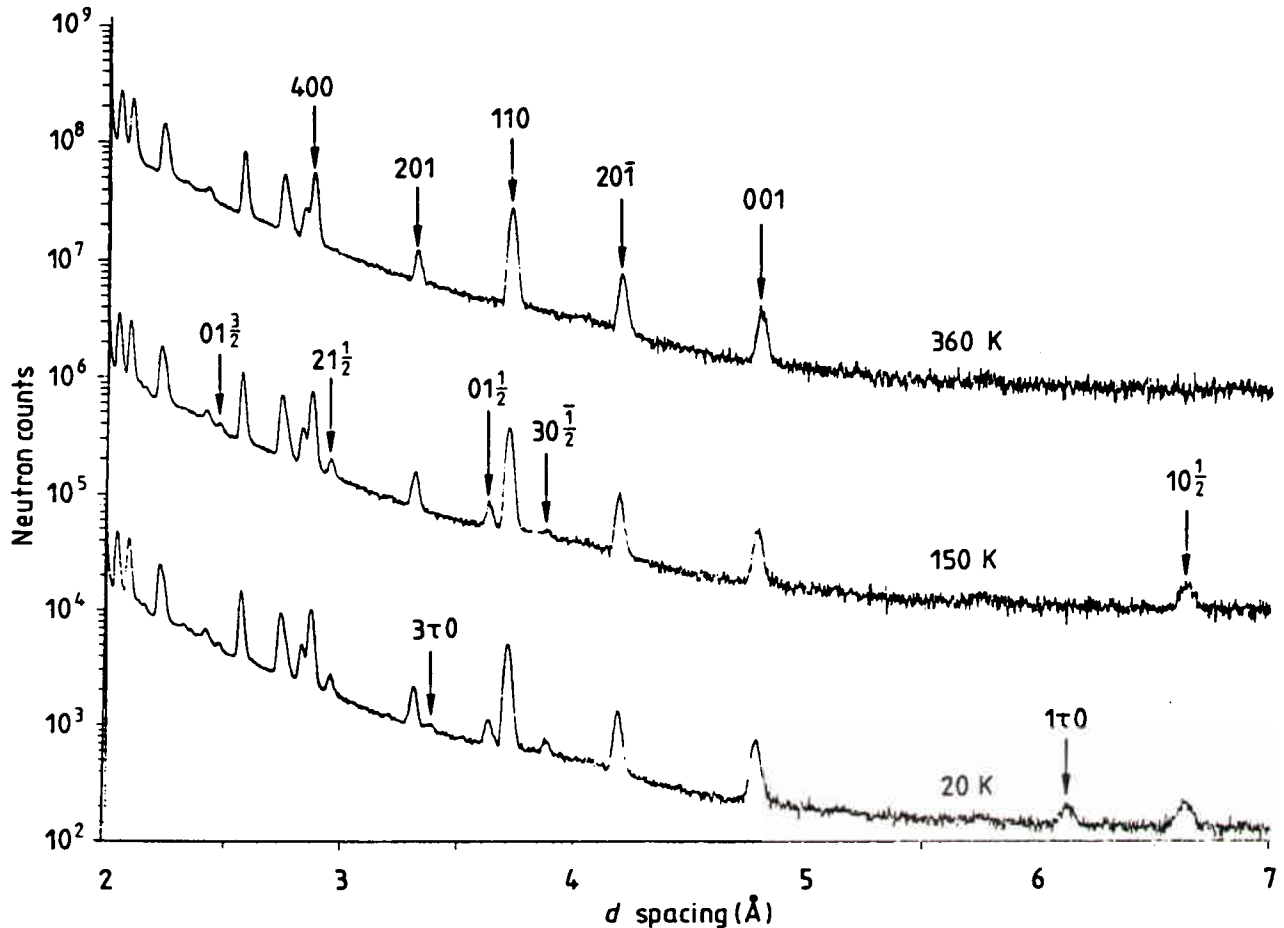


Figure 6. Raw time-of-flight diffraction data for FeGe at 360 K, 150 K, and 20 K taken with the $2\theta = 57^\circ$ detectors of the Special Environment Powder Diffractometer at IPNS. At each progressively lower temperature, only the new (magnetic) reflections are labelled. The data are plotted on a logarithmic scale ($\times 100$ for 150 K and $\times 10,000$ for 350 K) to make the large d spacings more visible since their raw intensities are reduced due to decreasing neutron flux at long wavelengths. (Reproduced from Ref. 11.)

temperature transition in SnMo_6S_8 and PbMo_6S_8 as the onset of a two-phase ($\overline{R}3 + \overline{P}1$) region (presumably resulting from grain interaction stresses) which is a precursor to the transition to the $\overline{P}1$ phase. Thus, the structural instability which results in the transition to a $\overline{P}1$ phase in EuMo_6S_8 and BaMo_6S_8 also exists in PbMo_6S_8 and SnMo_6S_8 , although the actual phase transition, which would result in a loss of superconductivity, is not reached in the latter compounds. The existence of the two-phase region, however, establishes that, at low temperature, SnMo_6S_8 and PbMo_6S_8 are adjacent to the phase line, leading to the conclusion that high- T_c superconductivity in these systems is related to the instability which gives rise to the symmetry-lowering transition.

Two-phase Rietveld refinements, such as the one shown in Fig. 7 for PbMo_6S_8 at 10 K, have established the structural parameters of the coexisting $\overline{R3}$ and $\overline{P1}$ phases and the phase fractions as a function of temperature.

2.2.4. Low-temperature structural ordering and superconductivity in the organic compounds $(\text{TMTSF})_2\text{X}$ and $(\text{BEDT-TTF})_2\text{X}$. Structural ordering has been shown to be intimately related to superconductivity in organic compounds. Low-temperature single crystal neutron diffraction techniques have played an important role in establishing the ordered structures. The structural ordering usually involves the X anion. In the case of $(\text{TMTSF})_2\text{ClO}_4$, which exhibits a T_c of 1 K, the ordering is commensurate and results in a cell doubling along the b axis.¹³ However, for $(\text{BEDT-TTF})_2\text{I}_3$, the ordering is incommensurate.¹⁴ The

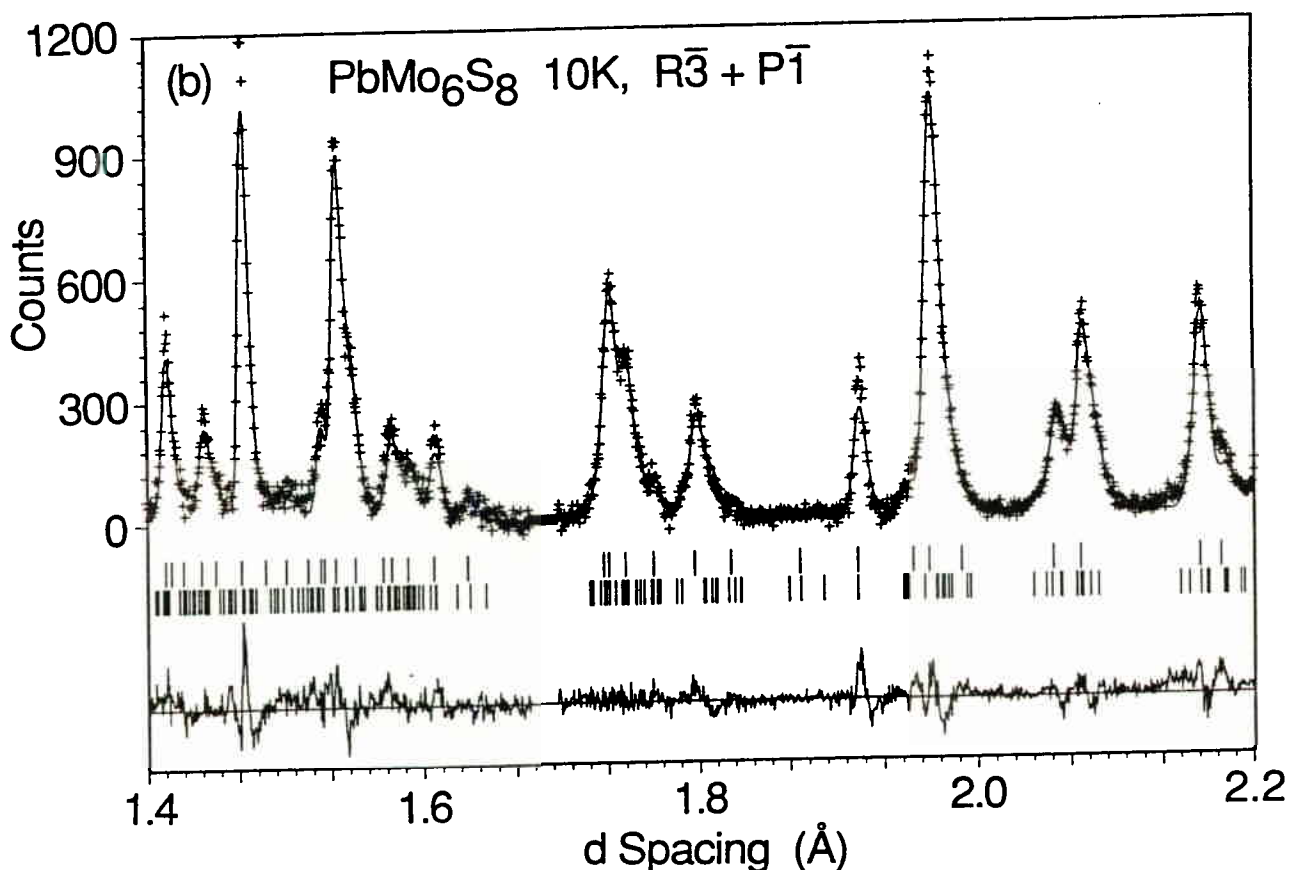


Figure 7. Portion of the Rietveld structural refinement profile based on a two-phase (rhombohedral $\overline{R3}$ plus triclinic $\overline{P1}$) model for PbMo_6S_8 at 10 K. Plus signs (+) are the raw data. The continuous line is the calculated profile. At the bottom of the curves, vertical tick marks indicate positions of allowed $\overline{R3}$ (upper tick marks) and $\overline{P1}$ (lower tick marks) reflections. (Reproduced from Ref. 12.)

single crystal time-of-flight Laue technique, which uses a two-dimensional position-sensitive detector, is especially well suited for such studies because new reflections are always seen regardless of their position in reciprocal space.¹⁵ Figure 8 shows a cut of reciprocal space containing the new incommensurate satellite peaks which are associated with the ordering of I_3 anions in $(BEDT-TTF)_2I_3$ at low temperatures.

3. NEUTRON DIFFRACTION AT HIGH TEMPERATURE

High temperature neutron diffraction capabilities extend to temperatures above 2500°C.¹⁶ Diffraction experiments are conducted at high temperature for number of reasons. Structural phase transitions occur in a number of systems. In some cases more than one transition occurs as a function of temperature. If the diffractometer count rate is sufficiently high, a large number of data separated by small increments in temperature can be collected in order to study the behavior in the region of the transition. In some cases, intermediate phases, which exist only over a narrow temperature range have been identified. Several examples of these types of measurements are given elsewhere in this book. (See the paper by J. Pannetier.)

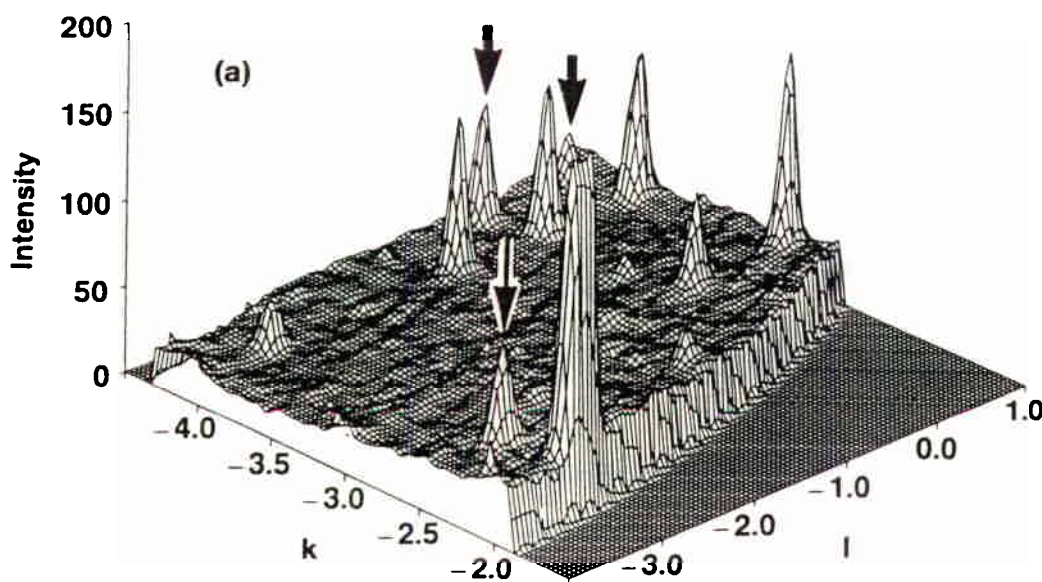


Figure 8. Plot of the time-of-flight neutron diffraction intensity in the $4.92, k, l$ reciprocal lattice plane of β - $(BEDT-TTF)_2I_3$ at 20 K. Satellite peaks at $(5, \bar{2}, \bar{3})-q$, $(5, \bar{4}, \bar{1})-q$, and $(5, \bar{4}, \bar{0})-q$ (marked with arrows) are clearly visible. (Figure adapted from Ref. 36.)

Neutron diffraction techniques have also been used to study chemical reactions as a function of time or temperature. Such studies have included hydration or dehydration reactions, intercalation, or reactions involving two separate chemical species. Again, for this type of work an instrument providing rapid data collection, with the entire pattern being collected simultaneously is required.

For several systems, diffraction data have been collected at high temperature in order to understand the structural features which are associated with other interesting high-temperature properties. For example, in the case of ionic conductors, it has been possible in some cases to identify structural changes which give rise to enhanced ionic conductivity at high temperature. In this context, it has also been possible to study the temperature-dependent creation of complex defects in systems such as nonstoichiometric metal oxides.

In some cases, high temperature diffraction measurements have been extended beyond the melting point into the liquid phase. Such measurements have provided particularly interesting results on the existence of specific local atomic configurations in liquid metals and melted glasses.

3.1. Experimental Methods

A wide range of furnace designs and heating techniques have been employed for neutron scattering experiments at high temperature at both steady state and pulsed neutron sources. In many cases, details of the furnace designs have been published. Although specific details of furnace geometry are too numerous to cover, all of the designs can be grouped into two general categories, and some general design criteria, particularly those which apply to time-of-flight neutron diffraction will be discussed.

Depending on the requirements of the sample, furnaces for neutron diffraction are either designed to operate with the sample in a vacuum or in a controlled atmosphere. In almost all cases, the heating element is in vacuum. Since the neutrons can easily penetrate the heating element and several concentric heat shields, beam attenuation is usually not a serious problem. However, particular care must be taken to avoid unwanted scattering from the furnace components surrounding the sample. This is usually accomplished through careful collimation or by leaving windows in the heating element and heat shields as shown in Fig. 1. Moving the heater and heat shields away from the sample is often not an acceptable solution since power requirements, and the overall heat load on the surroundings, go up markedly as the dimensions of the hot zone are increased. For this reason, time-of-flight techniques employing a single, fixed scattering angle can offer important advantages for high-temperature diffraction.

Several furnace designs are used routinely on the time-of-flight diffractometers at IPNS. For temperatures up to about 400°C, a simple aluminum can, with one heat shield, surrounding the sample (which is usually enclosed in a vanadium can) with windows for the straight-through beam (as in Fig. 1b) can provide perfectly clean data at all scattering angles with no beam attenuation.

For higher temperatures, a furnace without windows must be used in order to overcome undesirable losses and large thermal gradients in the hot zone. One successful design used at IPNS (designed and constructed by A. Howe and N. Wood, University of Leicester, U.K.) consists of a tubular heater and concentric heat shields made of thin vanadium. This furnace will reach temperatures of about 900°C and allows data collection at any scattering angle. Bragg scattering from the furnace is negligible, but the amount of vanadium in the beam is sufficient to contribute an amount of incoherent scattering which is larger than the normal sample background for many experiments.

Figure 9 shows a furnace design which maintains the sample in a controlled atmosphere. This furnace has been particularly useful for the study of high temperature oxides where the chemical stoichiometry is a function of the oxygen partial pressure of the atmosphere surrounding the sample. The sample is supported inside a closed-end aluminum oxide tube which contains a steady flow of the desired atmosphere. The heater is a spirally wound ribbon wound directly on the outer surface of the aluminum oxide tube in the original design, or onto a second closely-fitting concentric aluminum oxide tube in later designs. Since the aluminum oxide tube is close to the sample, scattering is limited to $2\theta = 90^\circ$ where collimation can be used to eliminate unwanted scattering from the furnace. The collimator is machined from boron nitride with windows for the incident beam and the scattered beam at $\pm 90^\circ$. Tantalum heat shields and zircar insulation are used outside the heat shield to

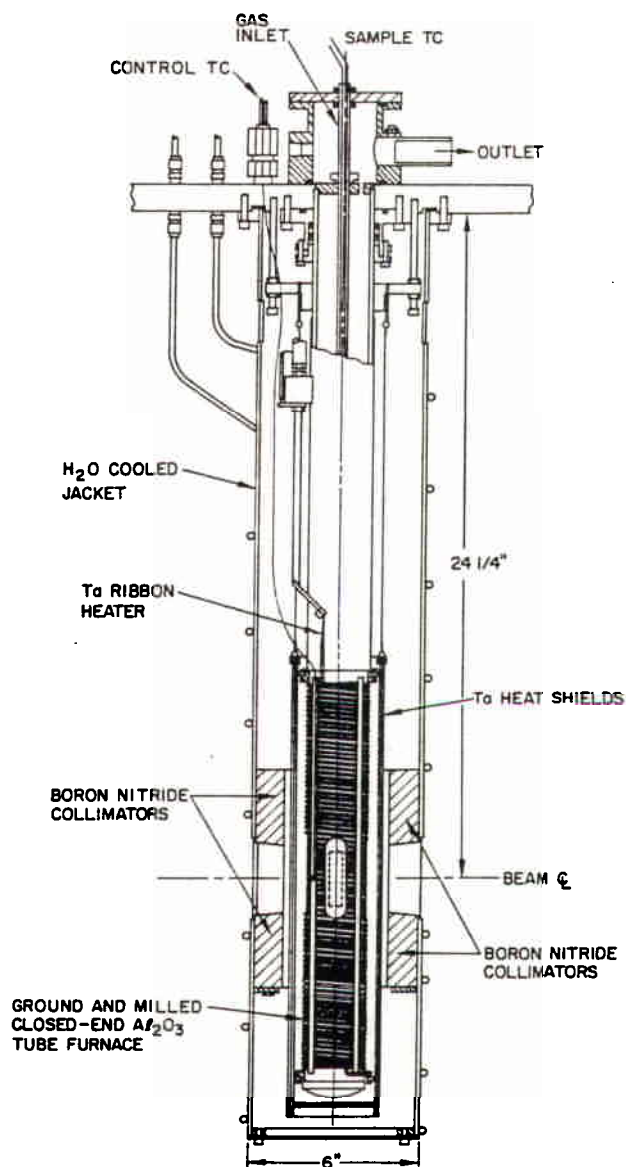


Figure 9. Schematic of the controlled-atmosphere, restricted angle ($2\theta = 90^\circ$) furnace used on the time-of-flight powder diffractometers at the Intense Pulsed Neutron Source.

minimize heat losses and to achieve a more uniform hot zone. The entire furnace is mounted inside a water-cooled jacket to control heat losses to surrounding instrument surfaces. This furnace design has been used successfully to temperatures of 1400°C, with approximately 2100 watts of input power.

3.2. Examples

The literature contains a number of high-temperature neutron diffraction experiments performed at both steady state and pulsed neutron sources. The highest temperature furnace designs presently operate at steady state sources where experiments have been performed at temperatures above 2500°C.¹⁷ The multidetector instrument D2B at ILL has also been used for a large number of high data rate experiments involving the study of phase transitions and reaction kinetics at lower temperature. These experiments are described elsewhere in these proceedings. (See the paper by J. Pannetier.) Although such experiments are not currently being done at pulsed sources, the time-of-flight technique also provides the fast, simultaneous data collection required for real-time experiments and will undoubtedly be used for such experiments in the future as appropriate experimental apparatus continues to be developed. In this paper two recent examples of high-temperature diffraction experiments performed at IPNS will be described.

3.2.1. Defects in CeO₂ versus temperature and composition. The controlled atmosphere furnace shown in Fig. 9 has been used to perform a number of experiments on metal oxides as a function of temperature and stoichiometry. For compounds which exhibit nonstoichiometric behavior, in situ experiments are required since quenching techniques are not always successful in freezing in the high-temperature state. In situ studies allow investigation of the equilibrium thermodynamic state in order to determine the structural and bonding properties and the atomic defects responsible for nonstoichiometric behavior.

Recent work on CeO_{2-x} provides an example of the kind of information that can be obtained from high-temperature neutron diffraction in a controlled atmosphere.¹⁸ In the case of CeO_{2-x} the oxygen stoichiometry can be varied over a range which includes the stoichiometric compound (0 < x < 0.2) by controlling the oxygen partial pressure surrounding the sample. Previous studies of nonstoichiometric CeO_{2-x} have shown that, when large vacancy defect concentrations are present, the oxygen ions displace from their ideal fluorite-structure sites towards neighboring interstitial cavities in the lattice. These displacements were attributed to the onset of complex defect interactions. A more recent study has concentrated on the stoichiometric compound CeO₂ produced by maintaining a pure oxygen atmosphere on the sample during neutron diffraction measurements to 1200°C. The powder diffraction data were analyzed in a model which includes third and fourth order terms in the Debye-Waller factor. Such an analysis is made possible by the existence of data to very short d spacings in the pulsed source experiment. These higher order terms in the Debye-Waller factors represent anharmonic displacements of the atoms. A plot of the

component of the symmetric third rank tensor, $C(ijk)$, that corresponds to cubic displacements of the oxygen atoms from their ideal fluorite positions versus temperature is shown in Fig. 10. The significant increase in this tensor component at high temperature corresponds to oxygen ion displacements toward the neighboring interstitial cavities, i.e., the same displacements that were previously seen as large static displacements in heavily defected samples. This suggests that the static displacements of atoms around oxygen vacancies are mediated by lattice phonons.

3.2.2. Oxygen atom positions in yttria-stabilized zirconia at high temperature and in an applied electric field. Nonstoichiometric oxides have also been investigated at high temperature by single crystal TOF neutron diffraction techniques. Figure 11 shows a simple furnace which was used to heat a single crystal of yttria-stabilized cubic zirconia.¹⁹ Data were collected at room temperatures and at 1040 K, with and without an electric field, on $Zr(y)O_{1.862}$ in an attempt to study the paths for

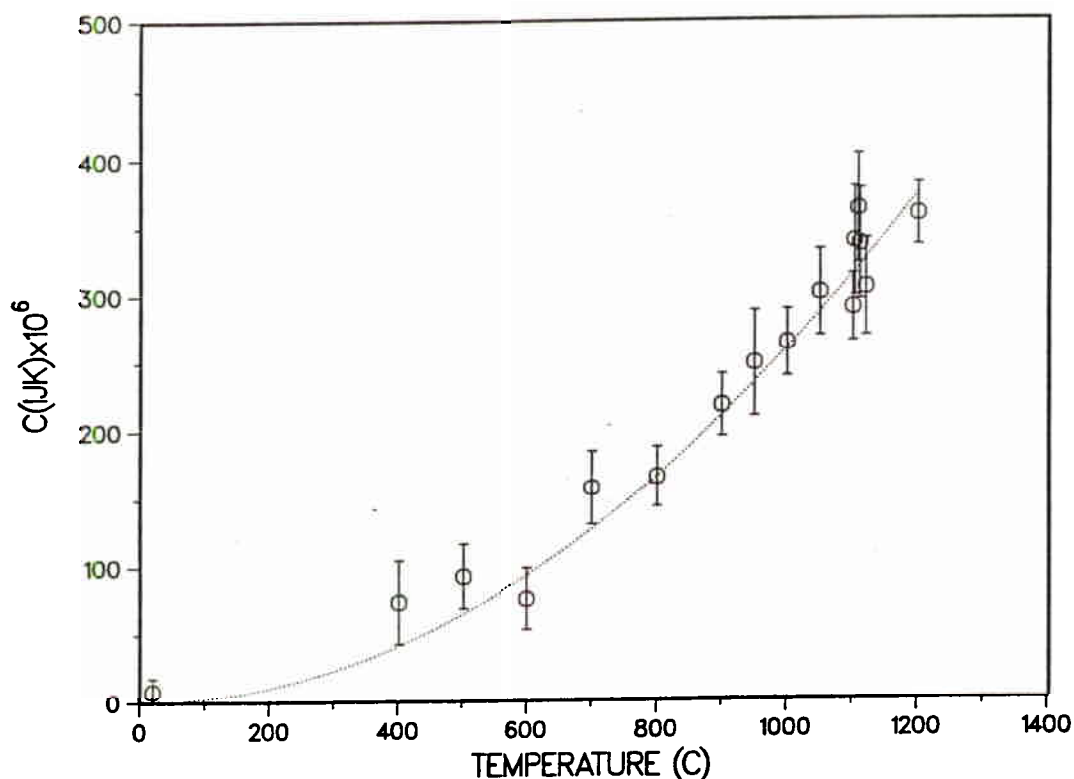


Figure 10. Component of the symmetric third rank tensor, $C(ijk)$, that corresponds to cubic displacements of the oxygen atom from their ideal fluorite positions in CeO_2 plotted as a function of temperature.

oxygen ionic motion leading to high ionic conductivity in this compound. Data for the sample in an electric field showed clear evidence for scattering density displaced from the oxygen sites in the $\langle 100 \rangle$ direction, thus suggesting that ionic current occurs with mobile O^{2-} ions moving along $\langle 100 \rangle$ directions through vacant oxygen sites.

4. NEUTRON DIFFRACTION AT HIGH PRESSURE

Neutron diffraction, and in particular the time-of-flight technique, has played a unique role in the area of high pressure.^{20,21} Since pressure cells necessarily have rather thick walls, a diffraction probe with high penetrating powder must be used. Additionally, in a high pressure

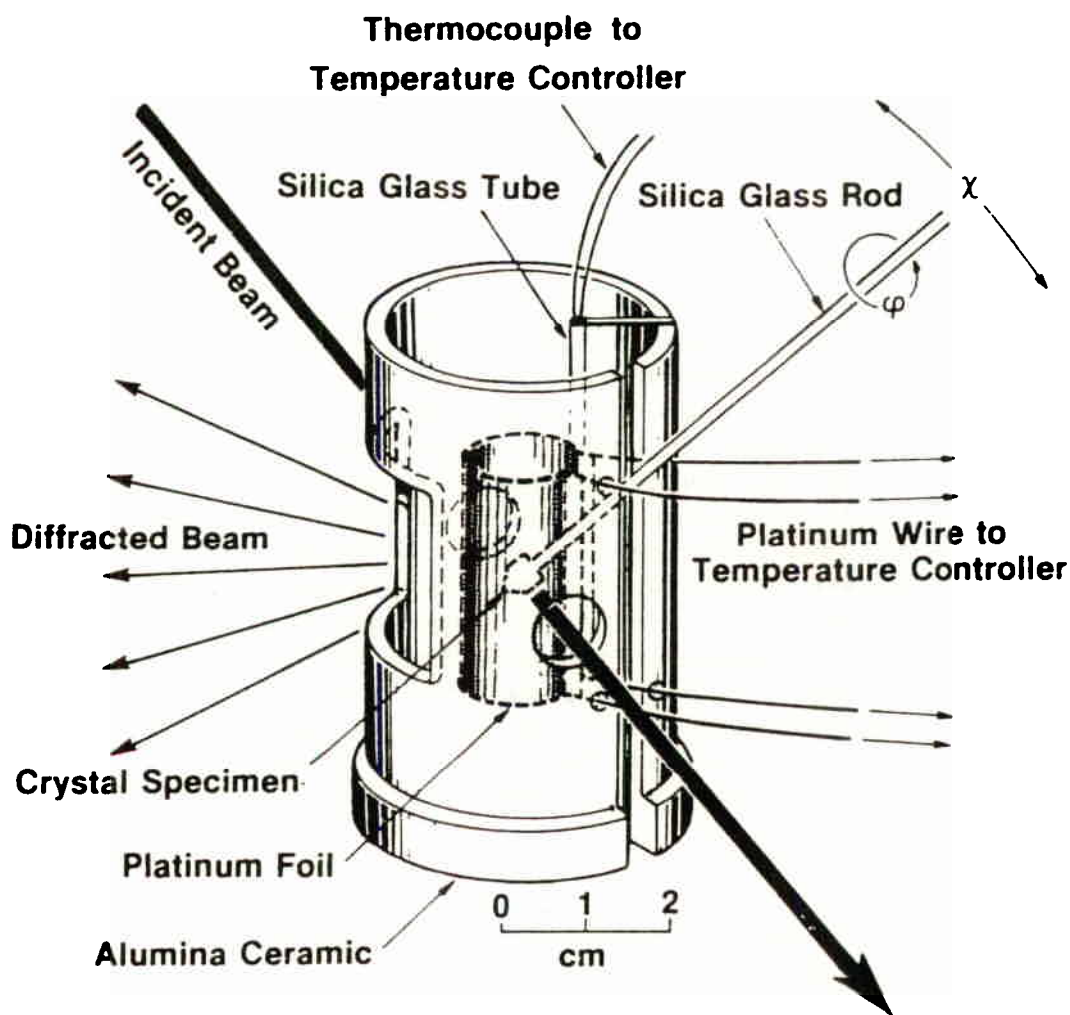


Figure 11. Furnace used for a time-of-flight single crystal neutron diffraction experiment on yttria-stabilized zirconia at high temperature and in an applied electric field. (Reproduced from Ref. 19.)

environment, the sample is supported by the walls of the pressure vessel. Thus, the time-of-flight, fixed-angle diffraction technique offers clear advantages for arranging collimation which will avoid scattering from the pressure vessel while maximizing scattering from the sample.

A number of interesting structural phenomena occur at high pressure. For most compounds the structural changes which occur at modest pressures are several times larger than those which can be produced by varying the temperature over the entire stability range of the compound. Thus, when the structural phase diagram for a compound is extended into the high pressure region, the number of different phases that are accessible is usually many times larger than the number which occur by varying temperature alone. Many of the high pressure studies in the literature report the determination of high pressure structures and the characterization of phase transitions as a function of pressure. Additionally, high pressure has become more common as a research tool for a wide range of other kinds of measurements, e.g., transport, elastic, and vibrational properties; and structural studies have been important in explaining other novel behavior observed at high pressure.

4.1. Experimental Methods

Because of strength limitations of the materials used to construct pressure cells, there exists an inverse relationship between the maximum pressure which can be achieved and the sample volume. These criteria presently limit the pressure at which routine neutron diffraction measurements can be done to about 40 kbar. The high pressure techniques most commonly used for neutron diffraction and the maximum pressure that can be achieved in each case are given in Table III. Gas pressure cells offer sample volumes as large as typical neutron diffraction samples (5 cm^3) and achieve perfectly hydrostatic pressure, even at low temperature, if helium is used as the pressure fluid.²² However, for safety reasons and because of the practical difficulty in achieving reliable helium seals at higher pressures, the use of helium gas cells for neutron diffraction has not been extended much beyond 8 kbar. Similar pressure cell designs, but with a suitable liquid for the pressure fluid, have been used to about 15 kbar.

TABLE III. High pressure techniques used for neutron scattering experiments.

<u>Method</u>	<u>Max. Pressure</u>
Gas cells	8 kbar
Liquid cells	15 kbar
Supported aluminum oxide cells	40 kbar

Beyond that pressure, the supported aluminum oxide cell is the design most often used for neutron diffraction measurements.^{20,23} Such a pressure cell, which has been used for many years to perform neutron diffraction measurements by the time-of-flight technique at both steady state and pulsed neutron sources, is shown in Fig. 12. This cell was originally developed in the late 1960's for high pressure structural measurements at the MTR Reactor in Idaho, where it was used with a chopper-based time-of-flight diffractometer. Even though the time-of-flight technique using a chopper on a reactor source is generally inferior to steady state techniques, the results achieved at high pressure were unique, owing to the ability to obtain data free from unwanted scattering from the pressure cell. The development of pulsed neutron sources has further enhanced this capability, allowing high pressure experiments with higher resolution and count rates.

The supported aluminum oxide design takes advantage of the high compressive strength of sintered aluminum oxide (approaching 500,000 psi for the best materials). A cylindrical sample is contained along with a

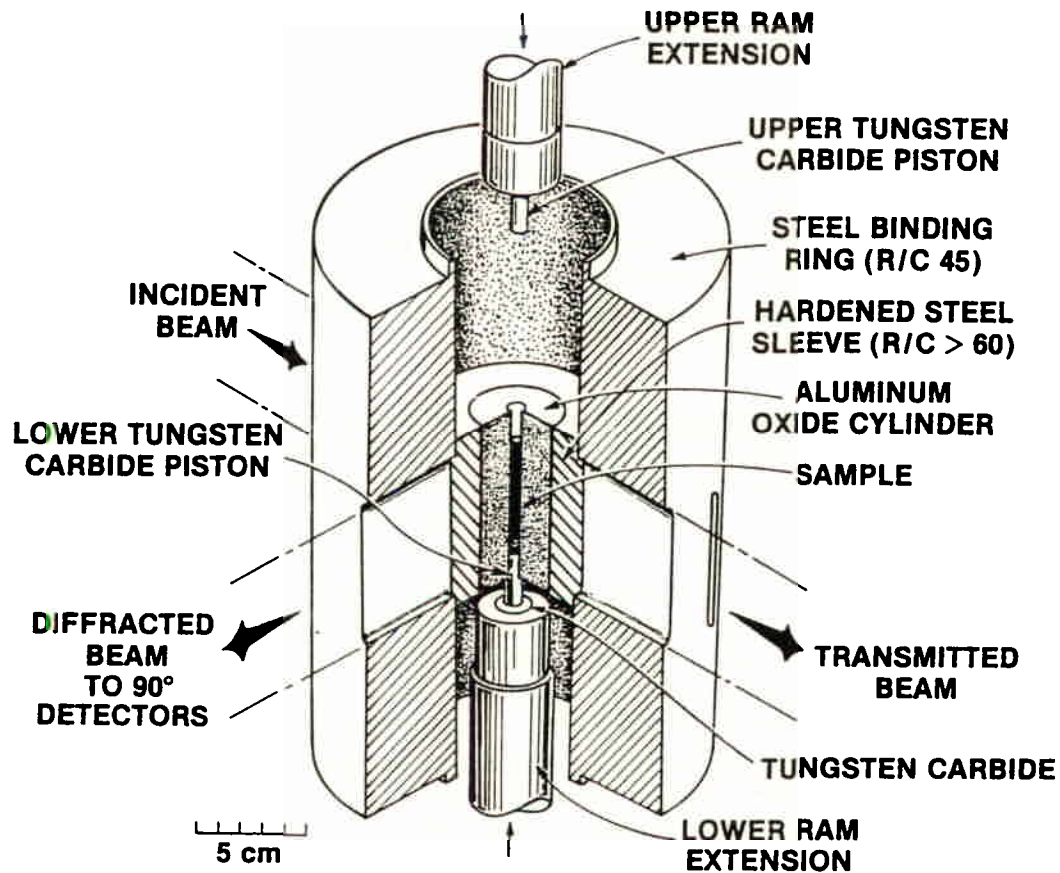


Figure 12. Supported aluminum oxide pressure cell used for time-of-flight neutron diffraction measurements at pressures to 40 kbar.

suitable hydrostatic fluid in a sealed capsule in the bore of a hollow aluminum oxide cylinder. The aluminum oxide cylinder is supported radially by one or more steel binding rings. Windows are cut in the steel, but not in the aluminum oxide, for the incident and scattered neutrons. In the case of the time-of-flight cell shown in Fig. 12, these windows also provide the desired collimation to mask scattering from the aluminum oxide. The neutrons must, of course, pass through the aluminum oxide. Typical attenuation factors are on the order of 50% for a total path of 2 cm of aluminum oxide. The cell is assembled in such a way that, with the sample at zero pressure, the aluminum oxide is at its compressive strength limit. In the design shown in Fig. 12, this is achieved by first loading the aluminum oxide cylinder into the hardened steel sleeve and then driving the sleeve, which is tapered, into the tapered bore of the steel binding ring. After assembling the cell in this way, as the sample pressure is increased, due to force applied to the ends of the sample capsule through tungsten carbide pistons, the compression in the aluminum oxide decreases and eventually passes through zero. The aluminum oxide then fails, by fracturing, when its tensile limit is reached. For typical designs this corresponds to a sample pressure of 40-50 kbar.

4.2. Examples

Even though high pressure neutron diffraction experiments are not as common as those performed at low or high temperature, the literature contains numerous examples and, additionally, several review articles on the subject.^{20,21} The examples cited here are from recent work at the Intense Pulsed Neutron Source and illustrate the current state of the art.

4.2.1. High pressure phases of ice. Ice is presently known to have at least eleven solid phases as a function of temperature and pressure. The structures of many of these phases were studied several years ago by neutron diffraction from samples which had been quenched from high pressure.²⁴⁻²⁶ Neutron diffraction, of course, allows the determination of the hydrogen atom positions so that the details of bonding can be studied. Not all of the ice phases, however, can be successfully quenched. During the last three years, there have been three papers reporting the structures of D₂O ice VI, VII, and VIII as determined by in situ neutron powder diffraction. The structure of ice VIII was refined from time-of-flight data taken at a reactor using the pressure cell shown in Fig. 12²⁷ while that of ice VII was determined using the same pressure cell at the Intense Pulsed Neutron Source.²⁸ Additionally, the structures of ices VI, VII, and VIII were studied in situ at the Institute Laue Langevin using fixed wavelength techniques.²⁹ These three recent papers provide a clear example of the relative merits of the three techniques. The two time-of-flight experiments both exhibit data free from pressure cell scattering, with the ice VII data having much higher resolution owing to the superior characteristics of the pulsed neutron source diffractometer. The data taken on the fixed wavelength instrument, by contrast, contained a large amount of Bragg

scattering from the aluminum oxide (Al_2O_3) pressure cell. This required an accurate subtraction of the Al_2O_3 pattern from the data in order to proceed with the analysis of the ice structures. A comparison of the data for D_2O ice VII taken by the two methods is shown in Fig. 13. The resulting answers from the data analysis were essentially identical, attesting to the skill of the ILL scientists in achieving an accurate pressure cell subtraction. However, the advantages of the time-of-flight technique are clearly illustrated and are essential for the refinement of more complex structures or for the solution of unknown structures.

4.2.2. Structure of high pressure KNO_3 -IV. One unknown high pressure structure recently solved from neutron powder diffraction data is that of KNO_3 -IV.³⁰ This phase of KNO_3 exists above about 3 kbar at room temperature. Data were collected at the Intense Pulsed Neutron Source with the sample in a helium gas pressure cell at 3.6 kbar. The unit cell was determined by autoindexing from a list of the d spacings of the observed Bragg peaks. The systematic absences required orthorhombic space group Pnma or its noncentrosymmetric equivalent. Atom locations were determined by attempting refinements of similar structures having the same space group chosen from the literature, until the correct model was found, and convergence of the Rietveld refinement was achieved. The high pressure structure is related to the atmospheric pressure structure in the novel way illustrated in Fig. 14. Both structures have the same orthorhombic Pnma symmetry. In the high pressure phase, the NO_3 molecules are displaced along the direction of the c-axis by an amount which results in a 26% reduction of the c-axis. This explains the large volume reduction associated with the KNO_3 -II to KNO_3 -IV transition.

4.2.3. "Compressibility collapse" transition in ReO_3 . Recent work on ReO_3 provides an instructive example of the use of both elastic and inelastic neutron scattering techniques to understand the pressure-induced phase transitions in ReO_3 . For this material, a continuous transition involving an order-of-magnitude increase in the compressibility was observed at 5 kbar.^{31,32} At atmospheric pressure ReO_3 has an ideal ABO_3 -type cubic perovskite structure with the A site being empty. It is well known that this structure can exhibit a number of structural instabilities leading to lower-symmetry or larger-cell structures. An obvious, but unproven, explanation for the large increase in compressibility was that the structure had undergone a transition to a symmetry in which coordinated rotations of the corner-linked ReO_6 octahedra could contribute to the cell compression.

This concept was first confirmed by a single crystal time-of-flight neutron diffraction experiment in which the ReO_3 $2a \times 2a \times 2a$ supercell with ReO_6 octahedra in rotated positions was observed.³³ Subsequently, inelastic neutron diffraction, performed at a reactor source, was used to observe the pressure-induced softening of the M-point phonon associated with the rotation of the ReO_6 octahedra.³⁴ In the final experiment, ReO_3 was studied by neutron powder diffraction over a range of pressures up to 27.4 kbar in order to investigate the order parameter and critical exponent of the transition.³⁵ The powder data revealed

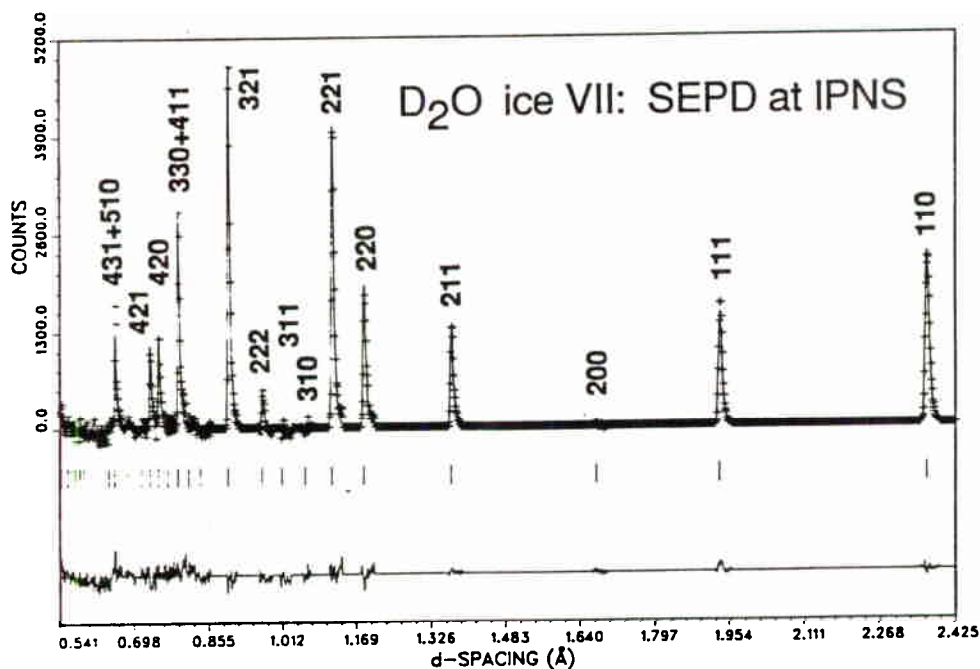
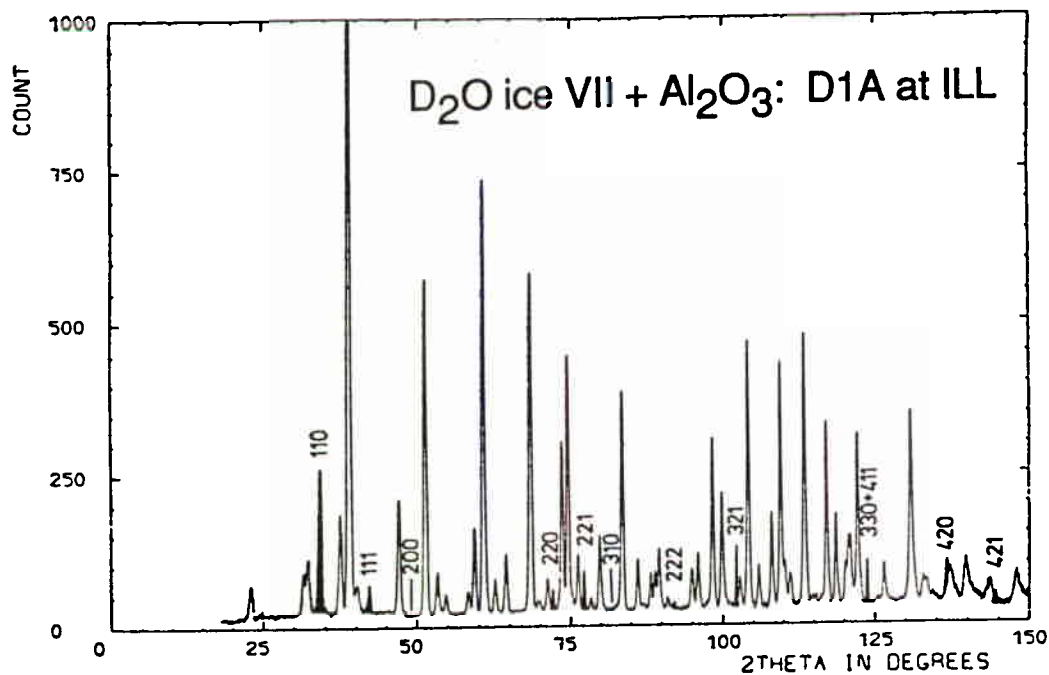
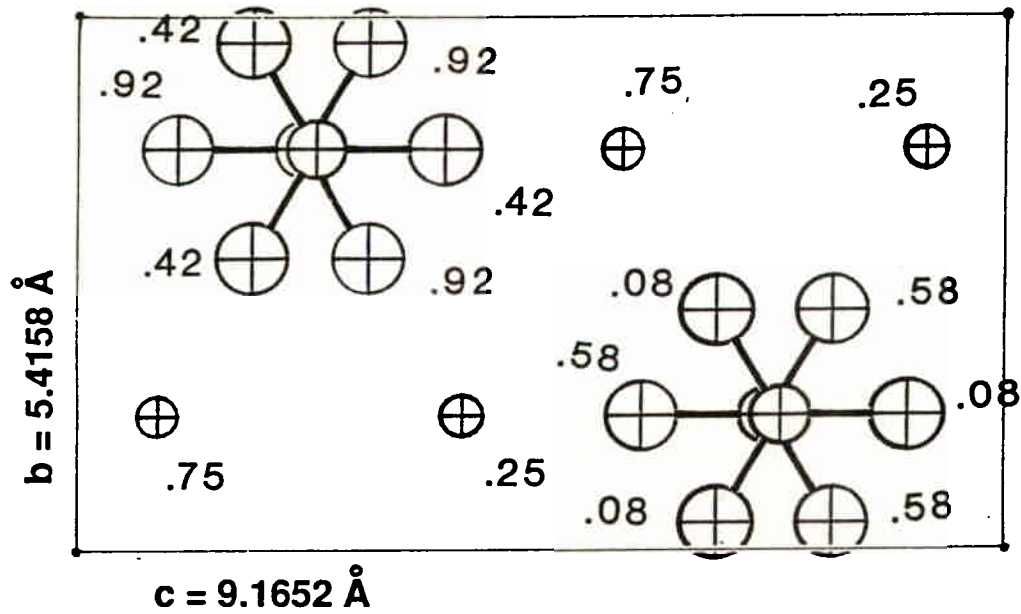


Figure 13. In situ neutron powder diffraction data for D₂O ice VII at approximately 25 kbar collected on the D1A fixed-wavelength diffractometer at ILL (top) and the SEPD time-of-flight diffractometer at IPNS (bottom). The D1A data show a large contribution of Al₂O₃ Bragg peaks from the pressure cell (the shaded peaks which are labelled with Bragg indices are the D₂O peaks in the D1A data). (Reproduced from Ref. 28 and 29.)

KNO₃-II (0 kbar, 295 K)



KNO₃-IV (3.6 kbar, 295 K)

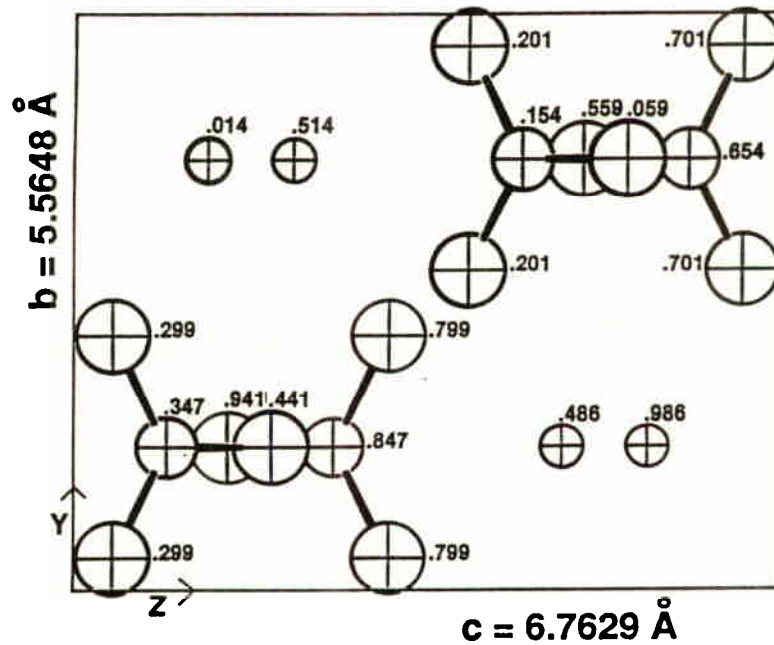


Figure 14. Comparison of the structures of KNO₃-II at atmospheric pressure and KNO₃-IV at 3.6 kbar. The largest symbols are O atoms and the smallest symbols are K atoms. Numbers near the atoms are fractional positions along the a axis. Both structures have orthorhombic Pnma space group symmetry (different origins are used in the two figures). Note how the NO₃⁻ ions slide past one another to substantially shorten the c axis in the high pressure KNO₃-IV structure.

that the system actually undergoes a series of transitions resulting from progressive softening of M-point phonons. The ReO_6 octahedra initially rotate round [001] axes, but as the pressure is further increased the axis of rotation shifts (in a first order transition that preserves cell volume) to [111]. The rotation angle, which is an order parameter for the transition, plotted as a function of pressure and fit to a power law yields the unusual critical exponent 0.322 ± 0.005 , as shown in Fig. 15.

4.2.4. Structural ordering and pressure-induced superconductivity in $(\text{BEDT-TTF})_2\text{I}_3$. The importance of structural ordering for superconductivity in organic compounds was discussed previously in section 2.2.4. In the case of $(\text{BEDT-TTF})_2\text{I}_3$, which exhibits a superconducting transition temperature of about 1.5 K, the ordering is incommensurate. More recent work has shown that the T_c of this compound suddenly jumps to about 8 K at a pressure of 0.5 kbar. The cause of this change in superconducting properties has been investigated by single crystal time-of-flight neutron diffraction at the Intense Pulsed Neutron Source.³⁶ At high pressure, the incommensurate satellite reflections shown in Fig. 8 are absent, indicating an even higher degree of ordering associated with the 8 K superconducting state.

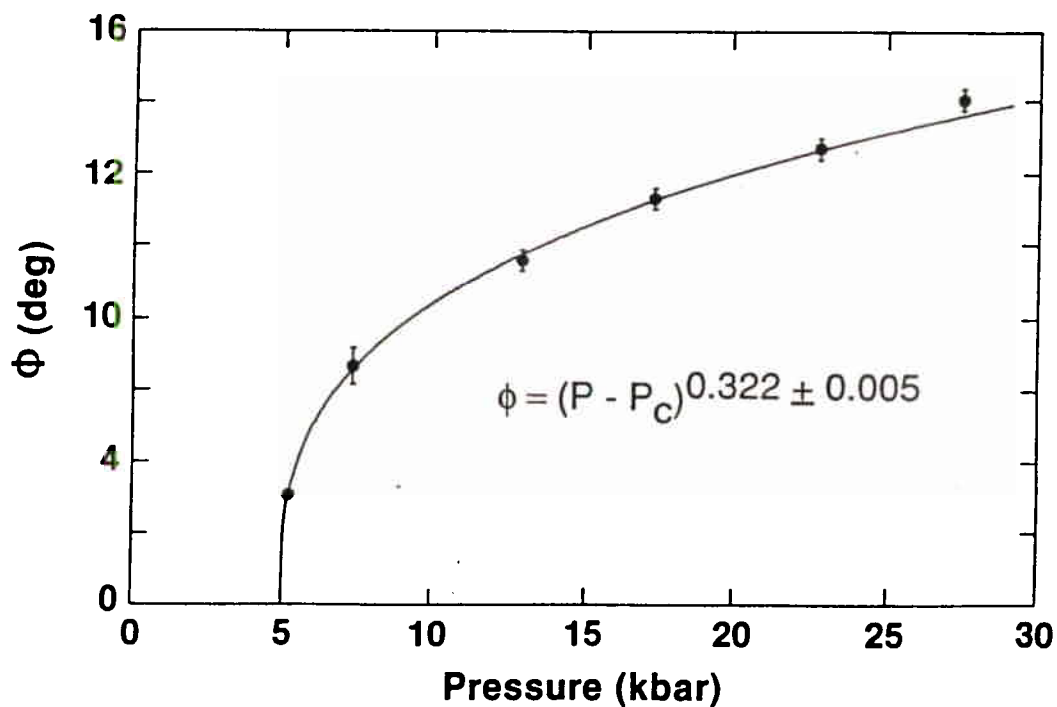


Figure 15. The rotation angle, ϕ , of ReO_6 octahedra in ReO_3 as measured by neutron powder diffraction plotted as a function of pressure. A power law fit to the data yields a critical exponent of 0.322 ± 0.005 . (Figure adapted from Ref. 35.)

5. SUMMARY

In this paper the general principles of neutron diffraction experiments in special sample environments have been discussed and illustrated with examples from the recent published literature. The discussion has focussed on low-temperature, high-temperature, and high-pressure techniques since these are routinely used at the major neutron scattering facilities. Space has not permitted inclusion of a discussion of more exotic techniques which could include sample environments such as steady-state or pulsed magnetic or electric fields, uniaxial compression or tensile stress, or in situ reaction vessels, but all of these techniques have been successfully used for neutron scattering experiments. Undoubtedly, the future will bring further developments, coupled with increased neutron flux and resolution at the advanced pulsed neutron sources that are now being proposed.

REFERENCES

1. The report of a recent meeting about special environment techniques for neutron scattering can be found in 'Proceedings of the Workshop on Sample Environments in Neutron and X-ray Experiments, Institut Laue-Langevin, Grenoble, France, Feb. 13-15, 1984,' *Revue Phys. Appl.* **19**, No. 9 (1984).
2. J. M. Carpenter, G. H. Lander, and C. G. Windsor, *Rev. Sci. Instrum.* **55**, 1019 (1984).
3. J. Faber, Jr., *Revue Phys. Appl.* **19**, 643 (1984).
4. P. A. Hilton and N. W. Kerley, *Revue Phys. Appl.* **19**, 775 (1984).
5. P. E. Sokol, R. O. Simmons, J. D. Jorgensen, and J. E. Jørgensen, *Phys. Rev. B* **31**, 620 (1985).
6. K. Sköld, C. A. Pelizzari, R. Kleb, and G. E. Ostrowski, *Phys. Rev. Lett.* **37**, 842 (1976).
7. W. G. Stirling, R. Scherm, P. A. Hilton, and R. A. Cowley, *J. Phys. C* **9**, 1643 (1976). P. A. Hilton, R. A. Cowley, R. Scherm, and W. G. Stirling, *J. Phys. C* **13**, L295 (1980).
8. A. Benoit, J. Bossy, J. Flouquet, and J. Schweizer, *J. Phys. Lett. (Orsay Fr.)* **46**, 923 (1985).
9. P. Roach, et al. (unpublished).
10. G. A. Lager, J. D. Jorgensen, and R. J. Rotella, *J. Appl. Phys.* **53**, 6751 (1982).
11. G. P. Felcher, J. D. Jorgensen, and R. Wapping, *J. Phys. C: Solid State Phys.* **16**, 6281 (1983).
12. J. D. Jorgensen, D. G. Hinks, and G. P. Felcher, *Phys. Rev. B* **35**, 5365 (1987).
13. P. C. W. Leung, A. J. Schultz, H. H. Wang, T. J. Emge, G. A. Ball, D. D. Cox, and J. M. Williams, *Phys. Rev. B* **30**, 1615 (1984).
14. T. J. Emge, P. C. W. Leung, M. A. Beno, A. J. Schultz, H. H. Wang, L. M. Sowa, and J. M. Williams, *Phys. Rev. B* **30**, 6780 (1984).
15. A. J. Schultz and P. C. W. Leung, *J. Physique* **47**, C5-137 (1986).
16. P. Aldebert, *Revue Phys. Appl.* **19**, 649 (1984).

17. K. Clausen, W. Hayes, M. T. Hutchings, J. E. Macdonald, and R. Osborn, *Revue Phys. Appl.* **19**, 719 (1984).
18. 'High temperature studies of stoichiometric cerium dioxide,' J. Faber, Jr. and R. L. Hitterman, *Proceedings of the Materials Research Society Meeting, Boston, Dec. 1-6, 1986 (in press)* and other unpublished work.
19. H. Horiuchi, A. J. Schultz, P. C. W. Leung, and J. M. Williams, *Acta Cryst. B* **40**, 367 (1984).
20. D. B. McWhan, *Revue Phys. Appl.* **19**, 715 (1984).
21. C. J. Carlile and D. C. Salter, *High Temp.-High Pressures* **10**, 1 (1978).
22. J. Paureau and C. Vettier, *Rev. Sci. Instrum.* **46**, 1484 (1975).
23. J. D. Jorgensen, *J. Appl. Phys.* **49**, 5473 (1978).
24. E. Walley, in Physics of Ice, edited by N. Riehl, B. Bullemer, and H. Engelhardt (Plenum Press, New York, 1969) p. 19.
25. B. Kamb, *Acta Cryst.* **17**, 1437 (1964).
26. S. J. LaPlaca and W. C. Hamilton, *J. Chem. Phys.* **58**, 567 (1973).
27. J. D. Jorgensen, R. A. Beyerlein, N. Watanabe, and T. G. Worlton, *J. Chem. Phys.* **81**, 3211 (1984).
28. J. D. Jorgensen and T. G. Worlton, *J. Chem. Phys.* **83**, 329 (1985).
29. W. F. Kuhs, J. L. Finney, C. Vettier, and D. V. Bliss, *J. Chem. Phys.* **81**, 3612 (1984).
30. T. G. Worlton, D. L. Decker, J. D. Jorgensen, and R. Kleb, *Physica B* **136**, 503 (1986).
31. B. Batlogg, R. G. Maines, and M. Greenblatt, in Physics of Solids Under High Pressure, edited by J. S. Schilling and R. N. Shelton (North Holland, 1981) p. 215.
32. B. Batlogg, R. G. Maines, M. Greenblatt, and S. DeGregorio, *Phys. Rev. B* **29**, 3762 (1984).
33. J. E. Schirber, B. Morosin, R. W. Alkire, A. C. Larson, and P. Vergamin, *Phys. Rev. B* **29**, 4150 (1984).
34. J. D. Axe, Y. Fujii, B. Batlogg, M. Greenblatt, and S. DeGregorio, *Phys. Rev. B* **31**, 663 (1985).
35. J.-E. Jorgensen, J. D. Jorgensen, B. Batlogg, J. P. Remeika, and J. D. Axe, *Phys. Rev. B* **33**, 4793 (1986).
36. A. J. Schultz, M. A. Beno, H. H. Wang, and J. M. Williams, *Phys. Rev. B* **33**, 7823 (1986).

DISCUSSION

HIGH PRESSURE WORK WITH SYNCHROTRON RADIATION

There is much interest in such work with diamond cells, but the latter cannot achieve a powder average and so are unsuitable for high quality powder experiments. Pressures can approach 1 Mbar. diffraction lines and hence phase changes can be seen, but intensities are unlikely to be reliable. The cubic anvil presses developed in Japan have a larger sample volume and have been used satisfactorily for high pressure work with synchrotron radiation. There will always be a place, however, for neutrons in high pressure studies.

ACCURACY OF NEUTRON INTENSITIES IN HIGH PRESSURE WORK

Measurement of the individual reflections in the study of potassium nitrate at 4 kbar shown above would require deconvolution of the overlapping ones, but an accuracy of about 3% should be possible for the best 20% of the reflections. The gas pressure cell contained a large volume sample and Rietveld refinement could be done to 1 - 2% expected statistics.

MEASUREMENT OF HIGH PRESSURES

Three techniques predominate. Gas pressure cells communicate with the pumping station by capillary, and the perfect fluidity of helium gas allows the pressure to be measured out of the pumping station by gauges with good accuracy. In the rhenium trioxide work the relation between volume and pressure was measured accurately by dilatometry in a separate experiment. For silica the pressure was determined by mixing a CsCl calibrant with the sample.

With a helium gas cell pressure and temperature changes can be reversed freely, but piston cylinder cells with Bridgeman seals are often not reversible.

USE OF PULSED NATURE OF NEUTRON BEAM

Very little use has so far been made of this aspect. Dr Jorgensen thought that pulsed neutron sources offered few advantages over reactors for time-resolved work, especially when the time-structure was shorter than the repetition rate. The pulse structure exists only at the source: at the sample the beam is instantaneously monochromatic and its wavelength varies with time.

